



## 1 Introduction

Magnetic resonance imaging (MRI) consists of a series of pulse sequences, *e.g.* T1-weighted (T1), contrast-enhanced (T1Gd), T2-weighted (T2), and T2-fluid-attenuated inversion recovery (Flair), each showing various contrast of water and fat tissues. The intensity contrast combination of multi-sequence MRI provides clinicians with different characteristics of tissues, extensively used in disease diagnosis [16], lesion segmentation [17], treatment prognosis [7], *etc.* However, some acquired sequences are unusable or missing in clinical settings due to incorrect machine settings, imaging artifacts, high scanning costs, time constraints, contrast agents allergies, and different acquisition protocols between hospitals [5]. Without rescanning or affecting the downstream pipelines, the MRI synthesis technique can generate missing sequences by leveraging redundant shared information between multiple sequences [18].

Many studies have demonstrated the potential of deep learning methods for image-to-image synthesis in the field of both nature images [12,11,8] and medical images [2,19,13]. Most of these works introduce an autoencoder-like architecture for image-to-image translation and employ adversarial loss to generate more realistic images. Unlike these one-to-one approaches, MRI synthesis faces the challenge of fusing complementary information from multiple input sequences. Recent studies about multi-sequence fusion can specifically be divided into two groups: (1) image fusion and (2) feature fusion. The image fusion approach is to concatenate sequences as a multi-channel input. Sharma *et al.* [18] design a network with multi-channel input and output, which combines all the available sequences and reconstructs the complete sequences at once. Li *et al.* [14] add an availability condition branch to guide the model to adapt features for different input combinations. Dalmaz *et al.* [9] equip the synthesis model with residual transformer blocks to learn contextual features. Image-level fusion is simple and efficient but unstable – zero-padding inputs for missing sequences lead to training unstable and slight misalignment between images can easily cause artifacts. In contrast, efforts have been made on feature fusion, which can alleviate the discrepancy across multiple sequences, as high-level features focus on the semantic regions and are less affected by input misalignment compared to images. Zhou *et al.* [23] design operation-based (*e.g.* summation, product, maximization) fusion blocks to densely combine the hierarchical features. And Li *et al.* [15] employ self-attention modules to integrate multi-level features. The model architectures of these methods are not flexible and difficult to adapt to various sequence combinations. More importantly, recent studies only focus on proposing end-to-end models, lacking quantifying the contributions for different sequences and estimating the qualities of generated images.

In this work, we propose an explainable task-specific fusion sequence-to-sequence (TSF-Seq2Seq) network, which has adaptive weights for specific synthesis tasks with different input combinations and targets. Specially, this framework can be easily extended to other tasks, such as segmentation. Our primary contributions are as follows: (1) We propose a flexible network to synthesize the target MRI sequence from an arbitrary combination of inputs; (2) The network

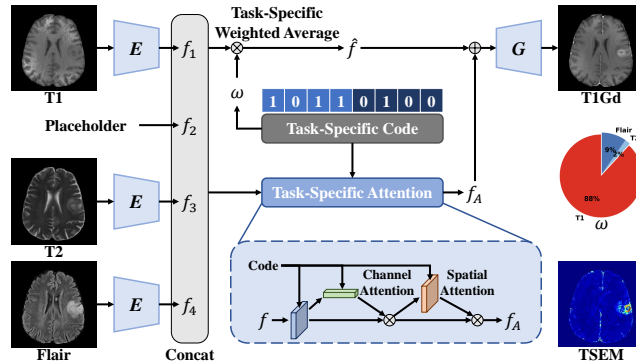


**Fig. 1.** Overview of the TSF-Seq2Seq network. By giving the task-specific code, TSF-Seq2Seq can synthesize a target sequence from existing sequences, and meanwhile, output the weight of input sequences  $\omega$  and the task-specific enhanced map (TSEM).

shows interpretability for fusion by quantifying the contribution of each input sequence; (3) The network provides reliability for synthesis by highlighting the area the network tried to refine.

## 2 Methods

Figure 1 illustrates the overview of the proposed TSF-Seq2Seq network. Our network has an autoencoder-like architecture including an encoder  $\mathbf{E}$ , a multi-sequence fusion module, and a decoder  $\mathbf{G}$ . Available MRI sequences are first encoded to features by  $\mathbf{E}$ , respectively. Then features from multiple input sequences are fused by giving the task-specific code, which identifies sources and targets with a binary code. Finally, the fused features are decoded to the target sequence by  $\mathbf{G}$ . Furthermore, to explain the mechanism of multi-sequence fusion, our network can quantify the contributions of different input sequences and visualize the TSEM.

To leverage shared information between sequences, we use  $\mathbf{E}$  and  $\mathbf{G}$  from Seq2Seq [10], which is a one-to-one synthetic model that integrates arbitrary sequence synthesis into single  $\mathbf{E}$  and  $\mathbf{G}$ . They can reduce the distance between different sequences at the feature level to help more stable fusion. Details of the multi-sequence fusion module and TSEM are described in the following sections.

### 2.1 Multi-Sequence Fusion

Define a set of  $N$  sequences MRI:  $\mathcal{X} = \{X_i | i = 1, \dots, N\}$  and corresponding available indicator  $\mathcal{A} \subset \{1, \dots, N\}$  and  $\mathcal{A} \neq \emptyset$ . Our goal is to predict the target set  $\mathcal{X}_{\mathcal{T}} = \{X_i | i \notin \mathcal{A}\}$  by giving the available set  $\mathcal{X}_{\mathcal{A}} = \{X_i | i \in \mathcal{A}\}$  and the corresponding task-specific code  $c = \{c_{\text{src}}, c_{\text{tgt}}\} \in \mathbb{Z}^{2N}$ . As shown in Fig. 1,  $c_{\text{src}}$  and

$c_{\text{tgt}}$  are zero-one codes for the source and the target set, respectively. To fuse multiple sequences at the feature level, we first encode images and concatenate the features as  $\vec{f} = \{\mathbf{E}(X_i) | i = 1, \dots, N\}$ . Specifically, we use zero-filled placeholders with the same shape as  $\mathbf{E}(X_i)$  to replace features of  $i \notin \mathcal{A}$  to handle arbitrary input sequence combinations. The multi-sequence fusion module includes: (1) a task-specific weighted average module for the linear combination of available features; (2) a task-specific attention module to refine the fused features.

**Task-Specific Weighted Average.** The weighted average is an intuitive fusion strategy that can quantify the contribution of different sequences directly. To learn the weight automatically, we use a trainable fully connected (FC) layer to predict the initial weight  $\omega_0 \in \mathbb{R}^N$  from  $c$ .

$$\omega_0 = \text{softmax}(c\mathbf{W} + \mathbf{b}) + \epsilon \quad (1)$$

where  $\mathbf{W}$  and  $\mathbf{b}$  are weights and bias for the FC layer,  $\epsilon = 10^{-5}$  to avoid dividing 0 in the following equation. To eliminate distractions and accelerate training, we force the weights of missing sequences in  $\omega_0$  to be 0 and guarantee the output  $\omega \in \mathbb{R}^N$  to sum to 1.

$$\omega = \frac{\omega_0 \cdot c_{\text{src}}}{\langle \omega_0, c_{\text{src}} \rangle} \quad (2)$$

where  $\cdot$  refers to the element-wise product and  $\langle \cdot, \cdot \rangle$  indicates the inner product. With the weights  $\omega$ , we can fuse multi-sequence features as  $\hat{f}$  by the linear combination.

$$\hat{f} = \langle \vec{f}, \omega \rangle \quad (3)$$

Specially,  $\hat{f} \equiv \mathbf{E}(X_i)$  when only one sequence  $i$  is available, *i.e.*  $\mathcal{A} = \{i\}$ . It demonstrates that the designed  $\omega$  can help the network excellently inherit the synthesis performance of pre-trained  $\mathbf{E}$  and  $\mathbf{G}$ . In this work, we use  $\omega$  to quantify the contribution of different input combinations.

**Task-Specific Attention.** Apart from the sequence-level fusion of  $\hat{f}$ , a task-specific attention module  $\mathbf{G}_A$  is introduced to refine the fused features at the pixel level. The weights of  $\mathbf{G}_A$  can adapt to the specific fusion task with the given target code. To build a conditional attention module, we replace convolutional layers in convolutional block attention module (CBAM) [20] with HyperConv [10]. As shown in Fig. 1, channel attention and spatial attention can provide adaptive feature refinement guided by the task-specific code  $c$  to generate residual attentional fused features  $f_A$ .

$$f_A = \mathbf{G}_A(\vec{f}|c) \quad (4)$$

**Loss function.** To force both  $\hat{f}$  and  $\hat{f} + f_A$  can be reconstructed to the target sequence by the conditional  $\mathbf{G}$ , a supervised reconstruction loss is given as,

$$\begin{aligned} \mathcal{L}_{rec} = & \lambda_r \cdot \|X' - X_{\text{tgt}}\|_1 + \lambda_p \cdot \mathcal{L}_p(X', X_{\text{tgt}}) \\ & + \lambda_r \cdot \|X'_A - X_{\text{tgt}}\|_1 + \lambda_p \cdot \mathcal{L}_p(X'_A, X_{\text{tgt}}) \end{aligned} \quad (5)$$

where  $X' = \mathbf{G}(\hat{f}|c_{\text{tgt}})$ ,  $X'_A = \mathbf{G}(\hat{f} + f_A|c_{\text{tgt}})$ ,  $X_{\text{tgt}} \in \mathcal{X}_{\mathcal{T}}$ ,  $\|\cdot\|_1$  refers to a  $L_1$  loss, and  $\mathcal{L}_p$  indicates the perceptual loss based on pre-trained VGG19.  $\lambda_r$  and  $\lambda_p$  are weight terms and are experimentally set to be 10 and 0.01.

## 2.2 Task-Specific Enhanced Map

As  $f_A$  is a contextual refinement for fused features, analyzing it can help us understand more what the network tried to do. Many studies focus on visualizing the attention maps to interpret the principle of the network, especially for the transformer modules [1,6]. However, visualization of the attention map is limited by its low resolution and rough boundary. Thus, we proposed the TSEM by subtracting the reconstructed target sequences with and without  $f_A$ , which has the same resolution as the original images and clear interpretation.

$$\text{TSEM} = |X'_A - X'| \quad (6)$$

## 3 Experiments

### 3.1 Dataset and Evaluation Metrics

We use brain MRI images of 1,251 subjects from Brain Tumor Segmentation 2021 (BraTS2021) [3,4,17], which includes four aligned sequences, T1, T1Gd, T2, and Flair, for each subject. We select 830 subjects for training, 93 for validation, and 328 for testing. All the images are intensity normalized to  $[-1, 1]$  and central cropped to  $128 \times 192 \times 192$ . During training, for each subject, a random number of sequences are selected as inputs and the rest as targets. For validation and testing, we fixed the input combinations and the target for each subject.

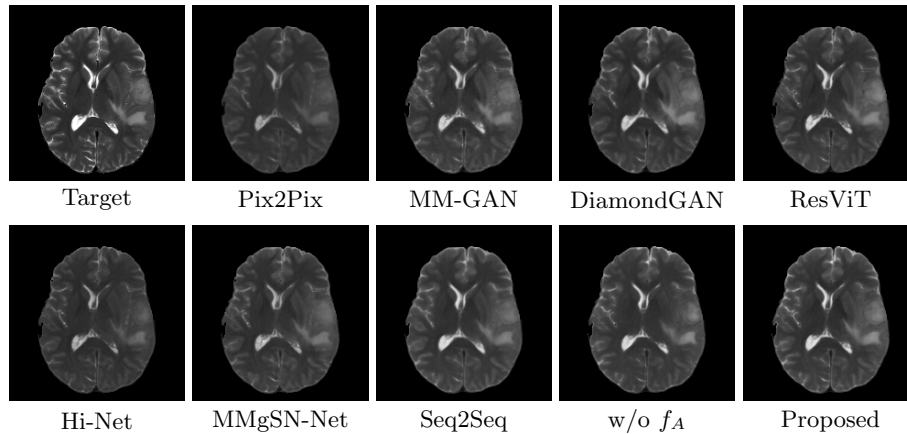


**Fig. 2.** Examples of synthetic T2 of comparison methods given the combination of T1Gd and Flair.

**Table 1.** Results for a set of sequences to a target sequence synthesis on BraTS2021.

Number of inputs	Methods	PSNR $\uparrow$	SSIM $\uparrow$	LPIPS $\downarrow$
1	Pix2Pix [12]	25.6 $\pm$ 3.1	0.819 $\pm$ 0.086	15.85 $\pm$ 9.41
	MM-GAN [18]	27.3 $\pm$ 2.4	0.864 $\pm$ 0.039	11.47 $\pm$ 3.76
	DiamondGAN[14]	27.0 $\pm$ 2.3	0.857 $\pm$ 0.040	11.95 $\pm$ 3.65
	ResViT [9]	26.8 $\pm$ 2.1	0.857 $\pm$ 0.037	11.82 $\pm$ 3.54
	Seq2Seq [10]	27.7 $\pm$ 2.4	0.869 $\pm$ 0.038	10.49 $\pm$ 3.63
	TSF-Seq2Seq (w/o $f_A$ )	27.8 $\pm$ 2.4	0.871 $\pm$ 0.039	<b>10.15<math>\pm</math>3.67</b>
	TSF-Seq2Seq	<b>27.8<math>\pm</math>2.4</b>	<b>0.872<math>\pm</math>0.039</b>	10.16 $\pm$ 3.69
2	Pix2Pix [12] (Average)	26.2 $\pm$ 2.7	0.834 $\pm$ 0.054	15.84 $\pm$ 6.05
	MM-GAN [18]	28.0 $\pm$ 2.3	0.878 $\pm$ 0.037	10.33 $\pm$ 3.58
	DiamondGAN[14]	27.7 $\pm$ 2.3	0.872 $\pm$ 0.038	10.82 $\pm$ 3.36
	ResViT [9]	27.7 $\pm$ 2.2	0.875 $\pm$ 0.035	10.53 $\pm$ 3.26
	Hi-Net [23]	27.1 $\pm$ 2.3	0.866 $\pm$ 0.039	11.11 $\pm$ 3.76
	MMgSN-Net [15]	27.1 $\pm$ 2.7	0.865 $\pm$ 0.044	11.38 $\pm$ 4.37
	Seq2Seq [10] (Average)	28.2 $\pm$ 2.2	0.879 $\pm$ 0.035	11.11 $\pm$ 3.72
	TSF-Seq2Seq (w/o $f_A$ )	28.0 $\pm$ 2.4	0.875 $\pm$ 0.039	9.89 $\pm$ 3.63
	TSF-Seq2Seq	<b>28.3<math>\pm</math>2.4</b>	<b>0.882<math>\pm</math>0.038</b>	<b>9.48<math>\pm</math>3.58</b>
3	Pix2Pix [12] (Average)	26.6 $\pm$ 2.5	0.842 $\pm$ 0.041	15.77 $\pm$ 5.08
	MM-GAN [18]	28.5 $\pm$ 2.5	0.883 $\pm$ 0.040	9.65 $\pm$ 3.57
	DiamondGAN[14]	28.2 $\pm$ 2.5	0.877 $\pm$ 0.041	10.20 $\pm$ 3.33
	ResViT [9]	28.3 $\pm$ 2.4	0.882 $\pm$ 0.039	9.87 $\pm$ 3.30
	Seq2Seq [10] (Average)	28.5 $\pm$ 2.3	0.880 $\pm$ 0.038	11.61 $\pm$ 3.87
	TSF-Seq2Seq (w/o $f_A$ )	28.3 $\pm$ 2.6	0.876 $\pm$ 0.044	9.61 $\pm$ 4.00
	TSF-Seq2Seq	<b>28.8<math>\pm</math>2.6</b>	<b>0.887<math>\pm</math>0.042</b>	<b>8.89<math>\pm</math>3.80</b>

The synthesis performance is quantified using the metrics of peak signal noise rate (PSNR), structural similarity index measure (SSIM), and learned perceptual image patch similarity (LPIPS) [21], which evaluate from intensity, structure, and perceptual aspects.

### 3.2 Implementation Details

The models are implemented with PyTorch and trained on the NVIDIA GeForce RTX 3090 Ti GPU. The **E** and **G** from Seq2Seq are pre-trained using the Adam optimizer with an initial learning rate of  $2 \times 10^{-4}$  and a batch size of 1 for 1,000,000 steps, taking about 60 hours. Then we finetune the TSF-Seq2Seq with the frozen **E** using the Adam optimizer with an initial learning rate of  $10^{-4}$  and a batch size of 1 for another 300,000 steps, taking about 40 hours.

### 3.3 Quantitative Results

We compare our method with one-to-one translation, image-level fusion, and feature-level fusion methods. One-to-one translation methods include Pix2Pix [12] and Seq2Seq [10]. Image-level fusion methods consist of MM-GAN [18], DiamondGAN [14], and ResViT [9]. Feature-level fusion methods include Hi-Net [23]

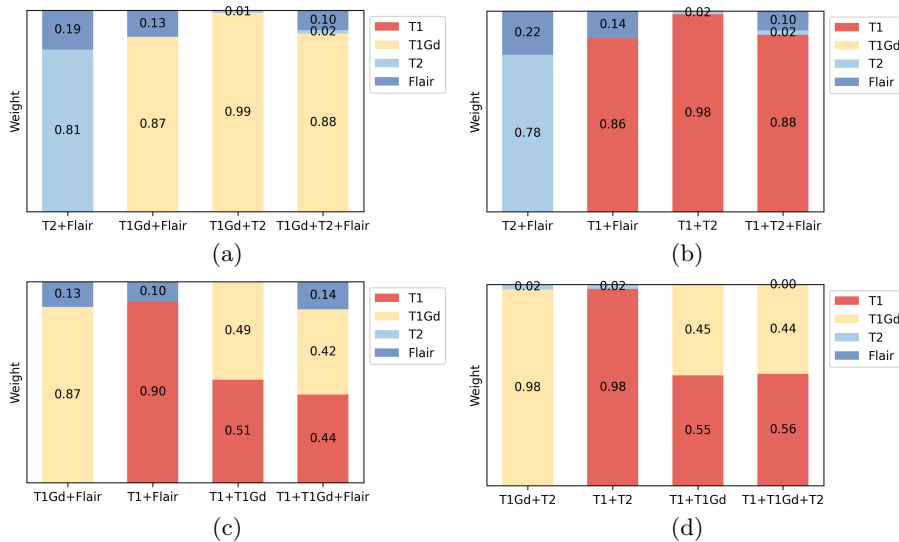


**Fig. 3.** Bar chart for the weights of the input set of sequences to synthesize different target sequences: (a) T1; (b) T1Gd; (c) T2; (d) Flair.

and MMgSN-Net [15]. Figure 2 shows the examples of synthetic T2 of comparison methods input with the combinations of T1Gd and Flair. Table 1 reports the sequence synthesis performance for comparison methods organized by the different numbers of input combinations. Note that, for multiple inputs, one-to-one translation methods synthesize multiple outputs separately and average them as one. And Hi-Net [23] and MMgSN-Net [15] only test on the subset with two inputs due to fixed network architectures. As shown in Table 1, the proposed method achieves the best performance in different input combinations.

### 3.4 Ablation Study

We compare two components of our method, including (1) task-specific weighted average and (2) task-specific attention, by conducting an ablation study between Seq2Seq, TSF-Seq2Seq (w/o  $f_A$ ), and TSF-Seq2Seq. TSF-Seq2Seq (w/o  $f_A$ ) refers to the model removing the task-specific attention module. As shown in Table 1, when only one sequence is available, our method can inherit the performance of Seq2Seq and achieve slight improvements. For multi-input situations, the task-specific weighted average can decrease LPIPS to achieve better perceptual performance. And task-specific attention can refine the fused features to achieve the best synthesis results.

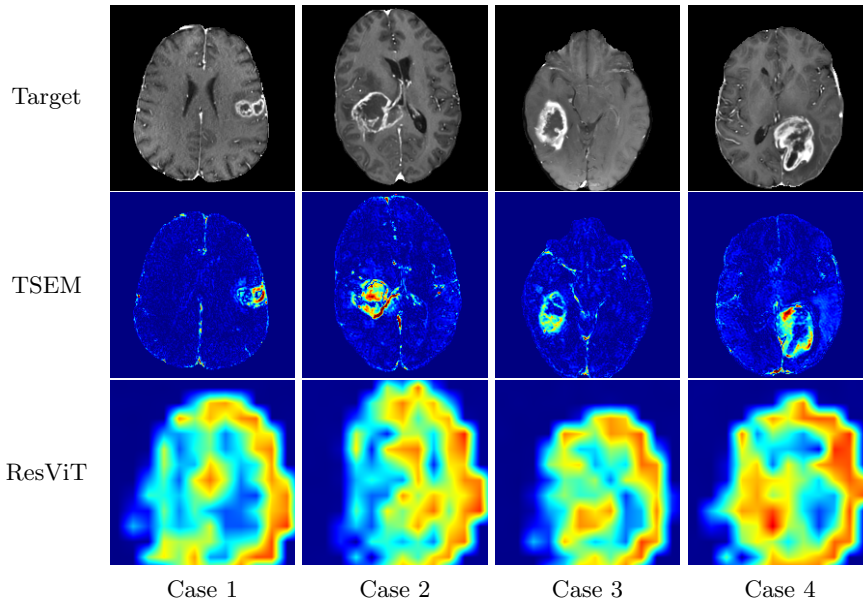


**Fig. 4.** Examples of the proposed TSEM and the attention maps extracted by ResViT [9] when generating T1Gd by given with T1, T2, and Flair.

**Table 2.** Results of PSNR for regions highlighted or not highlighted by TSEM.

Number of inputs	TSEM > 99%	TSEM < 99%	Total
1	18.0±3.2	28.3±2.4	27.8±2.4
2	18.8±3.7	28.8±2.4	28.3±2.4
3	19.5±4.0	29.3±2.5	28.8±2.6

### 3.5 Interpretability Visualization

The proposed method not only achieves superior synthesis performance but also has good interpretability. In this section, we will visualize the contribution of different input combinations and TSEM.

**Sequence Contribution.** We use  $\omega$  in Eq. 2 to quantify the contribution of different input combinations for synthesizing different target sequences. Figure 3 shows the bar chart for the sequence contribution weight  $\omega$  with different task-specific code  $c$ . As shown in Fig. 3, both T1 and T1Gd contribute greatly to the sequence synthesis of each other, which is expected because T1Gd are T1-weighted scanning after contrast agent injection, and the enhancement between these two sequences is indispensable for cancer detection and diagnosis. The less contribution of T2, when combined with T1 and/or T1Gd, is consistent with the clinical findings [23,22] that T2 can be well-synthesized by T1 and/or T1Gd.



**TSEM vs. Attention Map.** Figure 4 shows the proposed TSEM and the attention maps extracted by ResViT [9]. As shown in Fig. 4, TSEM has a higher resolution than the attention maps and can highlight the tumor area which is hard to be synthesized by the networks. Table 2 reports the results of PSNR for regions highlighted or not highlighted by TSEM with a threshold of the 99th percentile. To assist the synthesis models deploying in clinical settings, TSEM can be used as an attention and uncertainty map to remind clinicians of the possible unreliable synthesized area.

## 4 Conclusion

In this work, we introduce an explainable network for multi-to-one synthesis with extensive experiments and interpretability visualization. Experimental results based on BraTS2021 demonstrate the superiority of our approach compared with the state-of-the-art methods. And we will explore the proposed method in assisting downstream applications for multi-sequence analysis in future works.

## References

1. Abnar, S., Zuidema, W.: Quantifying attention flow in transformers. arXiv preprint arXiv:2005.00928 (2020)
2. Armanious, K., Jiang, C., Fischer, M., Küstner, T., Hepp, T., Nikolaou, K., Gatidis, S., Yang, B.: Medgan: Medical image translation using gans. *Computerized medical imaging and graphics* **79**, 101684 (2020)
3. Baid, U., Ghodasara, S., Mohan, S., Bilello, M., Calabrese, E., Colak, E., Farahani, K., Kalpathy-Cramer, J., Kitamura, F.C., Pati, S., et al.: The rsna-asnr-miccai brats 2021 benchmark on brain tumor segmentation and radiogenomic classification. arXiv preprint arXiv:2107.02314 (2021)
4. Bakas, S., Akbari, H., Sotiras, A., Bilello, M., Rozycki, M., Kirby, J.S., Freymann, J.B., Farahani, K., Davatzikos, C.: Advancing the cancer genome atlas glioma mri collections with expert segmentation labels and radiomic features. *Scientific data* **4**(1), 1–13 (2017)
5. Chartsias, A., Joyce, T., Giuffrida, M.V., Tsaftaris, S.A.: Multimodal mr synthesis via modality-invariant latent representation. *IEEE transactions on medical imaging* **37**(3), 803–814 (2017)
6. Chefer, H., Gur, S., Wolf, L.: Transformer interpretability beyond attention visualization. In: *Proceedings of the IEEE/CVF Conference on Computer Vision and Pattern Recognition*. pp. 782–791 (2021)
7. Chen, J.H., Su, M.Y.: Clinical application of magnetic resonance imaging in management of breast cancer patients receiving neoadjuvant chemotherapy. *BioMed research international* **2013** (2013)
8. Choi, Y., Choi, M., Kim, M., Ha, J.W., Kim, S., Choo, J.: Stargan: Unified generative adversarial networks for multi-domain image-to-image translation. In: *Proceedings of the IEEE conference on computer vision and pattern recognition*. pp. 8789–8797 (2018)
9. Dalmaz, O., Yurt, M., Çukur, T.: Resvit: residual vision transformers for multi-modal medical image synthesis. *IEEE Transactions on Medical Imaging* **41**(10), 2598–2614 (2022)

10. Han, L., Tan, T., Zhang, T., Huang, Y., Wang, X., Gao, Y., Teuwen, J., Mann, R.: Synthesis-based imaging-differentiation representation learning for multi-sequence 3d/4d mri. arXiv preprint arXiv:2302.00517 (2023)
11. Huang, X., Liu, M.Y., Belongie, S., Kautz, J.: Multimodal unsupervised image-to-image translation. In: Proceedings of the European conference on computer vision (ECCV). pp. 172–189 (2018)
12. Isola, P., Zhu, J.Y., Zhou, T., Efros, A.A.: Image-to-image translation with conditional adversarial networks. In: Proceedings of the IEEE conference on computer vision and pattern recognition. pp. 1125–1134 (2017)
13. Jung, E., Luna, M., Park, S.H.: Conditional gan with an attention-based generator and a 3d discriminator for 3d medical image generation. In: Medical Image Computing and Computer Assisted Intervention–MICCAI 2021: 24th International Conference, Strasbourg, France, September 27–October 1, 2021, Proceedings, Part VI 24. pp. 318–328. Springer (2021)
14. Li, H., Paetzold, J.C., Sekuboyina, A., Kofler, F., Zhang, J., Kirschke, J.S., Wiestler, B., Menze, B.: Diamondgan: unified multi-modal generative adversarial networks for mri sequences synthesis. In: Medical Image Computing and Computer Assisted Intervention–MICCAI 2019: 22nd International Conference, Shenzhen, China, October 13–17, 2019, Proceedings, Part IV 22. pp. 795–803. Springer (2019)
15. Li, W., Xiao, H., Li, T., Ren, G., Lam, S., Teng, X., Liu, C., Zhang, J., Lee, F.K.h., Au, K.h., et al.: Virtual contrast-enhanced magnetic resonance images synthesis for patients with nasopharyngeal carcinoma using multimodality-guided synergistic neural network. *International Journal of Radiation Oncology\* Biology\* Physics* **112**(4), 1033–1044 (2022)
16. Mann, R.M., Cho, N., Moy, L.: Breast mri: state of the art. *Radiology* **292**(3), 520–536 (2019)
17. Menze, B.H., Jakab, A., Bauer, S., Kalpathy-Cramer, J., Farahani, K., Kirby, J., Burren, Y., Porz, N., Slotboom, J., Wiest, R., et al.: The multimodal brain tumor image segmentation benchmark (brats). *IEEE transactions on medical imaging* **34**(10), 1993–2024 (2014)
18. Sharma, A., Hamarneh, G.: Missing mri pulse sequence synthesis using multi-modal generative adversarial network. *IEEE transactions on medical imaging* **39**(4), 1170–1183 (2019)
19. Uzunova, H., Ehrhardt, J., Handels, H.: Memory-efficient gan-based domain translation of high resolution 3d medical images. *Computerized Medical Imaging and Graphics* **86**, 101801 (2020)
20. Woo, S., Park, J., Lee, J.Y., Kweon, I.S.: Cbam: Convolutional block attention module. In: Proceedings of the European conference on computer vision (ECCV). pp. 3–19 (2018)
21. Zhang, R., Isola, P., Efros, A.A., Shechtman, E., Wang, O.: The unreasonable effectiveness of deep features as a perceptual metric. In: Proceedings of the IEEE conference on computer vision and pattern recognition. pp. 586–595 (2018)
22. Zhang, T., Tan, T., Han, L., Wang, X., Gao, Y., Teuwen, J., Beets-Tan, R., Mann, R.: Important-net: Integrated mri multi-parameter reinforcement fusion generator with attention network for synthesizing absent data. arXiv preprint arXiv:2302.01788 (2023)
23. Zhou, T., Fu, H., Chen, G., Shen, J., Shao, L.: Hi-net: hybrid-fusion network for multi-modal mr image synthesis. *IEEE transactions on medical imaging* **39**(9), 2772–2781 (2020)